Thermal Modeling of Absorber-Coupled TES Polarimeter

G. Wang[1], V. Yefremenko[1], A. Datesman[1], V. Novosad[1], J. Pearson[1], G. Shustakova[1, 6], R. Divan[2], J. Lee[3], C. L. Chang[4], J. McMahon[4], L. Bleem[4], A. T. Crites[4], T. Downes[4], J. Mehl[4], W. Everett[4], S. S. Meyer[4], J. E. Carlstrom[4], J. Sayer[5], and J. Ruhl[5]

[1]*Materials Science Division, Argonne National Laboratory, 9700 S Cass Ave., Argonne, IL 60439, USA*
[2]*Center for Nanoscale Materials, Argonne National Laboratory, 9700 S Cass Ave., Argonne, IL 60439, USA*
[3]*Advanced Photon Source, Argonne National Laboratory, 9700 S Cass Ave., Argonne, IL 60439, USA*
[4]*Kavli Institute for Cosmological Physics, the University of Chicago, 5640 S Ellis Ave., Chicago, IL 60637, USA*
[5]*Department of Physics, Case Western Reserve University, 10900 Euclid Ave., Cleveland, OH 44106, USA*
[6]*B. Verkin Institute for Low Temperature Physics and Engineering, Kharkov 61103, Ukraine*

Abstract. Using experimental thermal conductivity and volume heat capacity of narrow silicon nitride beams obtained from thermal test structures and a boundary limited phonon scattering model, as well as heat transport equation, we analyze thermal performance of an absorber-coupled polarimeter with finite element method. The polarimeter's temperature distribution, thermal power readout efficiency, and time constant are calculated. The TES thermal power readout efficiency of the polarimeter is up to 87% at a low signal modulation frequency, and has a 0.5 dB attenuation at 120Hz. We also compare a preliminary optical testing result with theoretical expectation.

Keywords: Bolometer, thermal conductance, superconducting detector, astrophysical instrumentation.
PACS: 07.57.Kp, 65.60.+a, 85.25.Pb, 95.55.-n.

INTRODUCTION

Bolometric polarimeter using a superconducting Transition Edge Sensor (TES) for the absorbed optical power readout is a sensitive receiver at millimeter and sub-millimeter wavelengths. The TES operating with a negative electro-thermal feedback has a fast response time and a low noise level [1-4]. The polarimeter has the desired performance for a sensitive observation of the Cosmic Microwave Background (CMB) radiation. The frontier of CMB research is to detect or to constrain the CMB B-mode polarization induced by inflationary gravitational waves at the very beginning of the universe [5, 6]. Furthermore, the polarization measurements of dusty high red-shift galaxies and of the gas and dust in the local universe at millimeter and sub-millimeter wavelengths have their own interest in astrophysics. Such measurements are used to investigate the magnetic field believed to be critical in the process of star formation [7-9].

We have been developing an absorber-coupled TES polarimeter for CMB B-mode detection. After a brief discussion of the design and fabrication of a prototype polarimeter, we present the thermal modeling of the polarimeter by using heat conduction equation, Finite Element Method (FEM), and experimental thermal parameters of narrow silicon nitride (Si_3N_4) beams. A primary testing result is compared with the modeling. The optical testing method of the polarimeter is presented separately [10].

DESIGN AND FABRICATION

The absorber-coupled polarimeter is designed for 95 GHz. It couples radiation from the sky through a feed horn into a 2.1 mm circular waveguide. The band-pass is defined at the low end by the waveguide cut-off and at the high end by a metal mesh low pass filter placed in front of the horn. The radiation in the waveguide is coupled to the TES through a half-wavelength absorber located on the center of the rectangular membrane which spans the guide $\lambda/4$ from a backshort. A waveguide choke prevents the fields from leaking out of the guide where the membrane penetrates. This design was optimized using High Frequency Structure Simulator (HFSS) to have a larger than 90% co-polar coupling and a less than 1% cross-

polar coupling [11]. The absorber and the TES are on a 1 μm thick rectangle, which is 3300 μm × 200 μm. Four 15 μm wide and two 25 μm wide Si_3N_4 beams support the rectangle and serve as a weak thermal link to the cryogenic heat bath. The length of the Si_3N_4 beams is 1.35 mm. The thermal conductance in the current layout is G≈200 pW/K. FIGURE 1 shows a completed polarimeter.

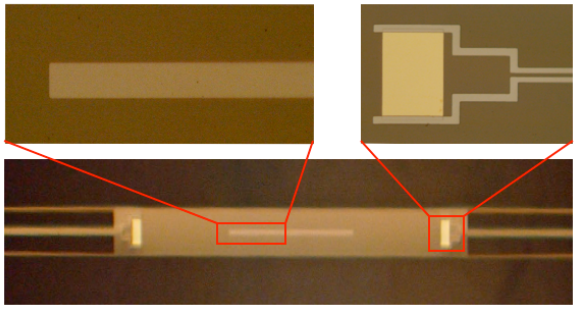

FIGURE 1. A 95 GHz absorber-coupled TES polarimeter. The absorber in the center is 1162 μm long and 18 μm wide. The separation between absorber and TES is 819 μm. Two 110 μm × 80 μm TESs are at the ends of the central rectangular Si_3N_4 membrane. Only one is used for readout. The Nb leads on the central beams connect TES to bias.

There is a detailed report of the polarimeter fabrication [12]. We only summarize the parameters used in the simulation. The Mo/Au bi-layer TES is made with DC magnetron sputtering and standard photolithography techniques. The Mo is 25 nm, and the Au is 30 nm. The 7 μm wide and 120 nm thick Nb leads are patterned with lift-off. The absorber, which consists of 3 nm Cr and 10 nm Au, is fabricated with DC magnetron sputtering and lift-off. The thickness of the absorber is chosen for a sheet impedance of 5.6 Ω/□ at the operating temperature for an optimized optical absorption.

THERMAL MODELING

The metal dipole of the polarimeter collects the electromagnetic waves polarized along the absorber. The optical power heats up the absorber and the entire Si_3N_4 rectangular membrane. The temperature change is then read out with a TES. The absorbed power eventually goes to the heat bath through the weak thermal link. We simulate the heat transfer of the polarimeter using FEM. The simulation provides the temperature distribution of the polarimeter at a constant optical power, as well as the TES temperature change with a modulated optical power on the top of the constant optical power when the TES is biased at a chosen voltage.

The heat conduction equation is

$$\nabla \cdot (\kappa \nabla T) + G_h = C_V \frac{dT}{dt}, \qquad (1)$$

where T is temperature, t is time, G_h is the heat source in units of W/cm^3, κ is temperature dependent thermal conductivity with units of W/cm·K, and C_V is temperature dependent volume heat capacity with units of J/cm^3·K.

There are two heat sources in the polarimeter: the optical power P_{OPT} and the TES Joule heating power P_J. We assume that the optical power is uniform in the absorber and the Joule heating power is uniform in the TES. With the TES in strong negative electro-thermal feedback, and using a small signal approximation, the TES Joule heating power is [1]

$$P_J = \left(\frac{V^2}{R_0}\right)\left(1 - \frac{\alpha}{T_0}(T - T_0)\right), \qquad (2)$$

where V is TES bias voltage, R_0 is the TES resistance at the operating point, T_0 is TES temperature with a constant optical power but without a modulated optical power, T is TES instant temperature with a modulated optical power, and α is defined as

$$\alpha = \left(\frac{T_0}{R_0}\right)\left(\frac{dR}{dT}\right)_{T=T_0}. \qquad (3)$$

The thermal parameters of the Si_3N_4 are found with the results of thermal conductance test structures [13]. In the experimental data of 1 μm thick Si_3N_4 beams, the thermal conductance ratio between 30 μm and 20 μm Si_3N_4 beams is 1.73 instead of 1.5, which is the beams cross section ratio. This result is interpreted with a boundary limited phonon scattering model [14]. We found that the average mean free path of phonons at the temperature between 0.30 K and 0.53 K is 11.1 (9.6) μm for the 30 (20) μm beams with a fraction of phonon diffusive reflection of 32% at surface. Using the measured thermal conductance data and the kinetic theory of phonons, we found that the Si_3N_4 volume heat capacity is $8.30\times10^{-8}T+5.09\times10^{-7}T^3$ J/cm^3·K. To apply the above results in the polarimeter thermal modeling, we assume the same fraction of diffusive reflection at surface and the same heat capacity of the Si_3N_4 beams. By extrapolation, the mean free path is 18.2 μm for 200 μm Si_3N_4 beams, 10.4 μm for 25 μm beams, and 8.6 μm for 15 μm beams. The thermal conductivity is calculated using $\kappa = C_V l S/3$, where C_V is volume heat capacity, l is phonon mean free path, and S=698600 cm/s is the average sound speed [15].

For both the absorber and the TES in its transition, we use metal thermal parameters [16], κ=0.2 W/cm·K and C_V=14.4×10^{-5} J/cm^3·K. The superconducting Nb leads contribute about 3% of volume of the support beams, and are treated as the same as 25 μm Si_3N_4 beams based on our testing results of the thermal conductance with various leads cross sections.

Equation (1) is solved in two dimensions for the polarimeter. However, Si_3N_4 membrane is treated as one layer, and the absorber and the TES are treated as a separate layer. The thermal coupling between the absorber and Si_3N_4 membrane, as well as between the TES and the Si_3N_4 membrane, is interpreted as electron phonon decoupling [17]. The thermal power exchange follows $P_{ep}=\Lambda\Sigma(T^5-T_{SiN}^5)$, where T is the temperature in the absorber or the TES, Λ=1×10^3 W/cm^3·K^5 is the coupling strength, and Σ is the absorber or the TES volume.

With a constant optical power P_{OPT}=16 pW, a TES operated at a resistance of R_0=0.5 Ω, a shunt resistance of 8.6 mΩ, and a TES bias voltage of 2.1 μV, the temperature distribution of the polarimeter at a steady state is shown in FIGURE 2.

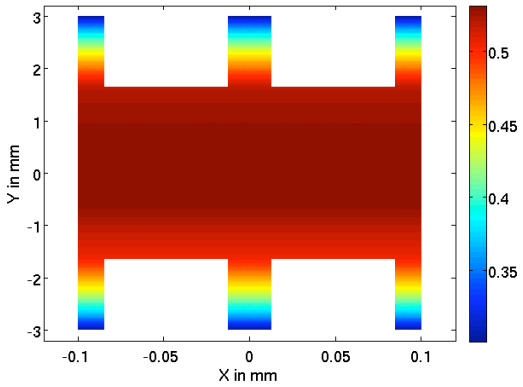

FIGURE 2. Temperature distribution of the polarimeter. The side bar is for temperature in K. The absorber has an average temperature of 0.534 K, the TES in use at the upper edge of the central rectangle has an average temperature of 0.524 K, and the TES not in use at the lower edge has an average temperature of 0.509 K. The temperature gradient is mainly on the narrow Si_3N_4 beams.

A modulated optical power on top of the constant optical power may be applied to the absorber, then the TES output is a function of the modulation frequency. The TES current change is proportional to its temperature change, $\Delta I=(V/R_0)(\alpha/T_0)(T-T_0)$. The readout efficiency of the polarimeter is the TES Joule heating power reduction, $\Delta P_J=(V^2/R_0)(\alpha/T_0)(T-T_0)$, divided by the modulation part of the optical power. FIGURE 3 shows the readout efficiency of the optical power as a function of the modulation frequency. It is assumed that the optical coupling efficiency to the absorber is 100% in the simulation. Therefore, the readout efficiency is purely thermal performance of the polarimeter. The least square fit gives a time constant τ=432 μs assuming the TES responsivity in the form of $R=A/\sqrt{(1+\tau^2\omega^2)}$, where A=0.87, $\omega=2\pi f$. The single pole fit slightly over-estimates the efficiency around 100 Hz and under-estimates the efficiency around 300 Hz.

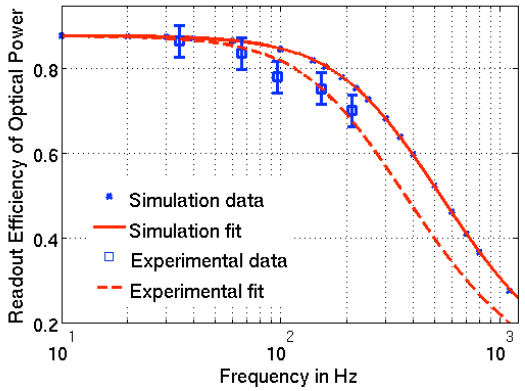

FIGURE 3. The TES readout efficiency of a modulated optical power in the absorber is a function of its modulation frequency. The 0.5 dB attenuation is at 120 Hz in the simulation, and is at 80 Hz in the experimental data fit.

We measured the Joule heating power readout efficiency of TES 1 at one end of the central rectangle by using TES 2 at the other end as a sensor in a dark test of a polarimeter which has a thermal conductance of G=1.3T$^{2.3}$ nW/K. TES 1 has a Tc=0.596 K and is connected to 4 wires. TES 2 has a Tc=0.637 K and is connected to a SQUID amplifier. At a bath temperature of 0.370 K, we found that TES 2 can read 76% Joule power of TES 1 by taking the I-V curves of TES 2 with various Joule powers on TES 1. This is compatible with the readout efficiency of the central absorber's thermal power using TES in the simulation if the heat source location difference is counted.

The thermal power readout efficiency reduction at a larger frequency is related to the heat transport time from the absorber to the TES and the relaxation time of the polarimeter. The interfacial thermal impedance between the absorber and the Si_3N_4 membrane gives a time constant less than 1 μs, which is negligible. The thermal diffusion time constant of Si_3N_4 membrane is $\tau_1=L^2/D$, where L is thermal diffusion length from the absorber to the TES, and $D=\kappa/C_V$ is thermal diffusivity of the Si_3N_4. We estimate $\tau_1\approx$30 μs using the thermal parameters in the simulation. Ideally, the TES, the absorber and the central rectangle are isothermal. Therefore, the TES time constant can be defined as $\tau_2=\tau_0/(1+\alpha\phi/n)$ [2], where $\tau_0=C_{det}/G$, $\phi=1-(T_{bath}/T_{tes})^n$, C_{det} is the detector's heat capacity, G is the thermal conductance between TES and the bath, α is defined in

(3), and we take n≈3 for the polarimeter with narrow Si_3N_4 beams as a weak thermal link. However, there is a temperature gradient in the central rectangle. The absorber, the central rectangle, and the support beams have a significant amount of heat capacity. We may write the relaxation time of the polarimeter approximately as $\tau_2=\Theta\tau_0/(1+\alpha\phi/n)$, where Θ is a scaling factor in characterization of the non-ideal thermal relaxation of the polarimeter. In the simulation, the polarimeter's thermal relaxation time constant is τ_2=402 μs. It's natural time constant $\tau_0\approx$1.26 ms, α=160, T_{bath}/T_{tes}=0.57, and the TES loop gain $\alpha\phi/3$=43.4, therefore, $\Theta\approx$14.1.

The time constant of a prototype polarimeter was investigated optically with a chopped external thermal source. The polarimeter has a thermal conductance of $G=0.85T^2$ nW/K. The TES, which has a transition temperature of 0.580 K and a normal resistance of 1.25 Ω, is operated at 1.0 Ω in its transition. The bath temperature is T_{bath}=0.520 K. The TES transition width is about 6 mK. A frequency multiplexing SQUID electronics is used for the TES current change readout. The data collection electronics has a digitization speed of one kilohertz, so we use the Fourier transformation amplitude at the chopping frequency to quantize the signal. The squares in FIGURE 3 are the testing data normalized to the simulation efficiency. The error bar is large due to the stability issue of low heat capacity polarimeter using narrow band readout electronics. The dashed line is a single pole fit, which has a time constant τ=625 μs. The time constant is larger than that in simulation. One reason is that the TES loop gain is smaller due to a higher bath temperature. The exact value of the TES α in the superconducting transition is not measured. Therefore, we cannot further compare the testing result with the simulation in terms of quantitative thermal parameters.

CONCLUSION

Starting with heat transport equation, we predict the thermal performance of an absorber-coupled TES polarimeter, such as its temperature distribution at a static state with a constant optical power and its optical power readout efficiency as a function of input signal modulation frequency. The thermal conductivity and volume heat capacity of tailored Si_3N_4 membrane of our thermal test structures are utilized in the simulation. Both the simulation and the testing result show that an absorber-coupled polarimeter has a bandwidth suitable for an astrophysical observation. Further work will be more polarimeters optical testing at a temperature required for observations for a thorough understanding of the polarimeter's dynamics and a comparison with the simulation.

ACKNOWLEDGMENTS

The authors wish to acknowledge the support from the NIST Quantum Sensors Group at Boulder for providing SQUID array, and to thank Matthew E. Kenyon at JPL for suggestions of devices fabrication. The work at Argonne National Laboratory, including the use of facility at the Center for Nanoscale Materials, was supported by the U.S. Department of Energy, under Contract No. DE-AC02-06CH11357. The work at the University of Chicago is supported by the National Science Foundation through grant ANT-0638937 and the NSF Physics Frontier Center grant PHY-0114422 to the Kavli Institute of Cosmological Physics at the University of Chicago. It also receives generous support from the Kavli Foundation and the Gordon and Betty Moore Foundation.

REFERENCES

1. S. W. Nam, *et al*., *IEEE Transactions on Applied Superconductivity* **9,** pp. 4209 (1999).
2. K. D. Irwin, *et al*., *Journal of Applied Physics* **83**, pp. 3978 (1998).
3. A. T. Lee, *et al. Applied Physics Letters* **69**, pp. 1806 (1996).
4. J. G. Staguhn, *et al*., *Nuclear Instruments and Methods in Physics Research A* **520**, pp. 336-339 (2004).
5. R. Crittenden, R. L. Davis, and P. J. Steinhardt, *The Astrophysical Journal* **417**, pp. L13-L16 (1993).
6. L. Page, *et al*., *The Astrophysical Journal Supplement Series* **170**, pp. 335 (2007).
7. J. M. Girart, R. Rao, and D. P. Marrone, *Science* **313**, pp. 812 (2006).
8. K. E. K. Coppin, *et al*., *Astronomy and Astrophysics* **356**, pp. 1031 (2000).
9. A. Lazarian and S. Prunet, *AIP. Conference series* **609**, pp. 32-43 (2002). Melville, New York, American Institute of Physics.
10. A. T. Crites*, et al.*, submitted to *LTD-13 Proceedings* (2009).
11. J. McMahon*, et al.*, submitted to *LTD-13 Proceedings* (2009).
12. V. Yefremenko*, et al.*, submitted to *LTD-13 Proceedings* (2009).
13. G. Wang, *et al*., submitted to *CEC-ICMC proceedings* (2009).
14. M. N. Wybourne, *et al., Journal of Physics C: Solid State Physics* **17**, pp. L607-L612 (1984).
15. R. J. Bruls, *et al*., *Journal of the European Ceramic Society* **21**, pp. 263-268 (2001).
16. F. Pobell, *Matter and Methods at Low Temperatures*, Springer, Berlin, 2007, pp. 33-93.
17. A. M. Savin, *et al*., *Journal of Applied Physics* **99**, pp. 084501 (2006).